WP1 result summary report relevant for "Environmental Best Practice"

Deliverable number 1.2

Tamara Baumberger[1], Stefan Bünz[2], Rolf B. Pedersen[1], Ann E. Blomberg[1,3], Karin Landschulze[1], Alexandros Tasianas[2], Christian Berndt[4], Jens Karstens[4], Holger Class[5], Waqas Ahmed[5], Bernd Flemisch[5], Andy Chadwick[6], Sam Holloway[6], James C. White[6], Melis Cevatoglu[7], Jonathan Bull[7], Bogdan Orlic[8]

1 – University of Bergen (UiB), Norway
2 – University of Tromsø (UiT), Norway
3 – University of Oslo (UiO), Norway
4 –GEOMAR Helmholtz Centre for Ocean Research Kiel (Geomar), Germany
5 – University of Stuttgart (UStutt), Germany
6 – British Geological Survey (BGS), UK
7 – National Oceanography Center, University of Southampton (N%2#ʒ . / #ĭ3 / 4 / .)
8 – TNO, Netherlands

05.11.2014


ECO2
Sub-seabed CO2 Storage:
Impact on Marine Ecosystems

Contents D1.2/ECO_2

Objectives **3**

1 Techniques and technologies for the characterization of the shallow overburden **3**
1.1 AUV / seafloor mapping 3
1.1.1 High-resolution interferometric synthetic aperture sonar (HISAS 1030) on an AUV 3
1.1.2 Seafloor mapping with hull-mounted echosounders 5

1.2 High-resolution & conventional 3D seismics 6
1.2.1 High-resolution 3D seismic – P-cable 6
1.2.2 Conventional 3D seismic 7

2 Strategies for baseline studies **8**
2.1 Leakage structures and pathways 8
2.1.1 Seafloor features, paleo-channels 8
2.1.2 Gas accumulation – bright spots 10
2.1.3 Vertical seal-bypassing fluid conduits – Seismic chimneys 11
2.1.4 Gas hydrates 12
2.1.5 Faults 13
2.1.6 Other stratigraphic structures promoting fluid flow 15

2.2 Leakage assessment 18
2.2.1 Leakage scenarios 18

3 Strategies for monitoring the shallow overburden **19**
3.1 Seafloor and shallow overburden 19
3.2 Overburden between sedimentary overburden and seafloor 20

4 Modeling strategies to support leakage assessment **22**
4.1 Geological Model 23
4.2 Conceptual Model 24
4.3 Mathematical & Numerical Model 24
4.4 Validation 24
4.5 Application 25
4.6 HW-Lattice-Boltzmann Model 27

References **29**

Appendix **31**

Objectives

This report will provide a best practice approach to characterizing the architecture and integrity of a storage site and provide a catalogue of possible leak scenarios with an estimate of their likelihood of occurrence.

This report will provide information about the best strategies for monitoring the shallow overburden.

1 Techniques and technologies for the characterization of the shallow overburden

1. 1 AUV / seafloor mapping

1.1.1 High-resolution interferometric synthetic aperture sonar (HISAS 1030) and other acoustic and chemical survey instruments on an AUV

Marine basic science investigations as well as marine applied studies strongly depend on the knowledge of the topographic characteristics of the seafloor. Until recently, multibeam echo-sounder systems and sidescan sonars were the most advanced technique to map the seafloor. The newly developed AUV mounted high-resolution synthetic aperture sonar (HISAS) opened a new era in seafloor mapping and imaging.

The HISAS 1030 sonar system is an advanced interferometric sidescan sonar developed by Kongsberg Maritime. It consists of a transmitter and two vertically displaced receiver arrays configured as an interferometer. The HISAS is capable of synthetic aperture sonar (SAS) imaging, resulting in a range independent obtainable image resolution better than 5x5 cm (max. 2x2 cm, depending on the conditions). High-resolution bathymetric maps are obtained by compositing the interferometric product between the two vertically offset receive arrays. While technically range invariant the system normally provides a 400 m swath. The HISAS frequency range is approximately 60 to 120 kHz, with a bandwidth of 30-50 kHz (Fossum et al., 2008).

The HISAS, in combination with the AUV Hugin, was several times successfully used for detailed imaging of the seafloor. Deployed in June 2011, a fracture in the seafloor was discovered in the North Sea by using the HISAS mounted on Hugin. It was not possible to identify this fracture by conventional seafloor mapping using the multibeam echo-sounder system. The fracture was subsequently named after the vehicle – Hugin Fracture. The central and eastern part of the Hugin Fracture, imaged by using the HISAS, is shown here (Figure 1).

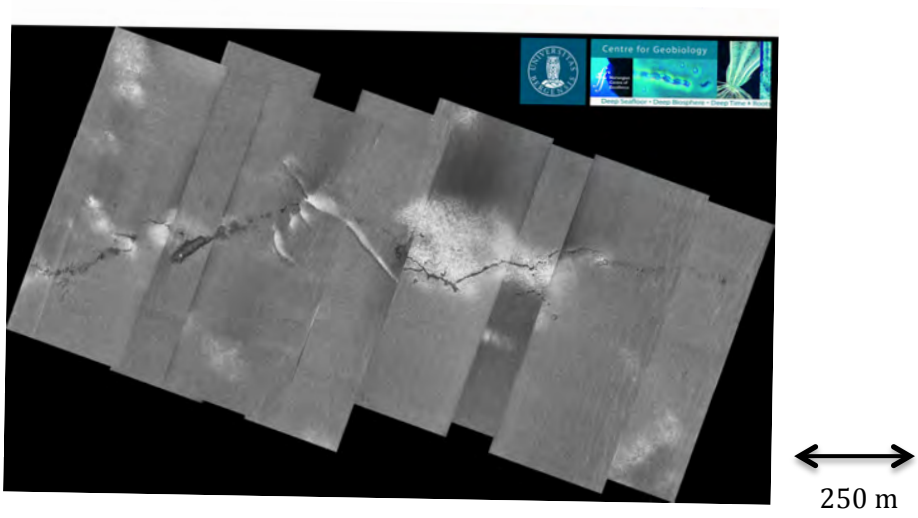

Figure 1: Central and eastern part of the Hugin Fracture, imaged by using the HISAS.

Advantages of this commercially available system is certainly the possibility for detailed imaging with a high resolution (better than 5x5 cm) out to 200 m from both sides of the vehicle and the high area coverage rates (typically 2 km^2/h) given the resolution achieved. Nevertheless, the system requires high navigational accuracy. Additionally, surface properties, steep topography, flocculent layers or bacterial mats can adversely influence the systems range and reception.

To investigate the Hugin Fracture in September 2012, a multidisciplinary Autosub 6000 dataset comprising active acoustics, Eh, pH, pCO_2 sensors and digital colour camera data was collected during JC077 cruise (University of Southampton), together with geochemical analyses of sediment and water samples. Autosub 6000 is an unmanned, 5.5 m long underwater vehicle, with depth rating up to 6000 m. By means of the acoustic telemetry and tracking system, the location of Autosub 6000 is detected precisely, proved during various test deployments. In current marine surveys, the operational speed is c. 2 m/s, during which Autosub 6000 has been found to successfully control its depth above the seabed. It is equipped with a Kongsberg Simrad EM 2000 multibeam bathymetric mapping system, as well as an Edgetech 2200-M Modular Sonar System for seismic reflection and side scan data acquisition. Several sensors are actually mounted on Autosub 6000, including Eh, pH and LSS sensors, as well as ADCP current profiler and a 5 M colour camera.

Eh sensor data has shown geochemical anomalies associated with this fault, suggesting lower levels of oxygen and sulphate for the fluids leaking from this fracture. Bacterial mats were also imaged by bottom photography, confirming fluid flow activity along this fault. The seabed is predominantly composed of sandy sediments, corresponding to low backscatter regions (grey areas) on the side-scan data. In addition, many shell hashes were imaged within the survey area, corresponding to high backscatter regions on the side-scan map, confirmed by bottom photography. Seabed infrastructure crossing the overall survey area, as well as dredging traces on the south are also observed on the side-scan map. The only fault detected within the survey area is the Hugin Fracture, and there is no evidence of a linked surface fault network from the present dataset in this area.

1.1.2 Seafloor mapping with hull-mounted echosounders

Multibeam echosounders (MBES) and single-beam echosounders (SBES) are potent tools to image both the water column and seabed. SBES have been used for many years in fisheries research, and can be used to identify the presence/absence of bubbles within a typical 10 degree beam footprint. MBES systems are used to collect high-resolution seafloor profiles across a swath typically 2-2.5x the water depth. Multibeam systems can also be used to acquire water column information, giving the full 3d shape of rising bubble plumes and fish schools.

Bathymetry is typically collected using a MBES. The R/V G.O. Sars, R/V James Cook, and R/V Alkor have an EM302, EM710, and Seabeam 1000 respectively. All of these MBES systems are fully capable within the depth range of 100 m to 1000 m applicable to this project. Proper technique in acquisition, quality assessment, and processing is essential to the creation of an accurate MBES data product. The key factors contributing to a quality survey are: the sound velocity profile, monitoring of the acquisition software, and grid-wide crossing lines for syn-acquisition reference.

The most important factor in the collection of acoustic soundings is the sound velocity profile (SVP). The sound structure informs ray-tracing algorithms in the acquisition software, and is used in real-time to accept or reject soundings used by the bottom-lock algorithms. In the open ocean the SVP is relatively stable, and a single CTD or expendable bathythermograph (XBT) deployment at the beginning of a survey is more than sufficient to acquire quality data. In places with complex topography, especially in regions of high relief with respect to the surrounding terrain, the SVP may only be stable for a matter of hours. Knowledge of the region to be surveyed is essential to estimate the frequency of SVPs that will need to be collected.

The limitations on collecting acoustic data vary by vessel, acquisition system, and the level of care used in setting up a survey. The most common limitation on acquisition is the co-collection of MBES, SBES, and sub-bottom profiling while performing survey work. In some instances, especially when a timing delay slave-master system is used, successful SBES and MBES data can be collected without degrading the data quality of either system. This however is rare, as purposeful monitoring of the acquisition systems requires skilled personnel onboard and working during the survey. Typically MBES and SBES systems are run concurrently, mutually interfering with each other and degrading the image and signal quality of the respective systems. This provides marked challenges to subsequently process the data, and in some cases makes identification of water column features in the MBES impossible due to the level of interference. That said, interaction of MBES and SBES typically does not damage the MBES signal to the point that it interferes with the collection of bathymetric data, though this is possible.

It is not possible to concurrently run a sub-bottom profiler and either MBES or SBES and collect high quality data on either of the latter systems. On the ships used during these investigations the R/V G.O. Sars and R/V Alkor both have parametric subbottom profilers. Parametric systems are acoustically very powerful, and completely destroy the STN ratio of any other echosounder running concurrent to subbottom profiler acquisition. For any useable MBES data to be collected, it must be run entirely independent of a subbottom parametric system to obtain a high quality of data collected.

1.2 High-resolution & conventional 3D seismics

1.2.1 High-resolution 3D seismic – P-cable

The P-Cable 3D high-resolution seismic system consists of a seismic cable towed perpendicular (cross cable) to the vessel's steaming direction. An array of multi-channel streamers is used to acquire many seismic lines simultaneously, thus covering a large area with close in-line spacing in a cost efficient way (Figure 2). The cross-cable is spread by two paravanes that due to their deflectors attempt to move away from the ship. The P-Cable system is designed and developed as a tool for marine geological research and the petroleum industry. It may be used in both frontier and mature regions in an intelligent, versatile way to acquire successive small-size surveys (25 to 250 km^2) in areas of special interest, e.g. 4D seismic monitoring of the shallow overburden at CO_2 storage sites. This is due to the fast deployment and recovery of the P-Cable and the short turns needed between adjacent sailing lines.

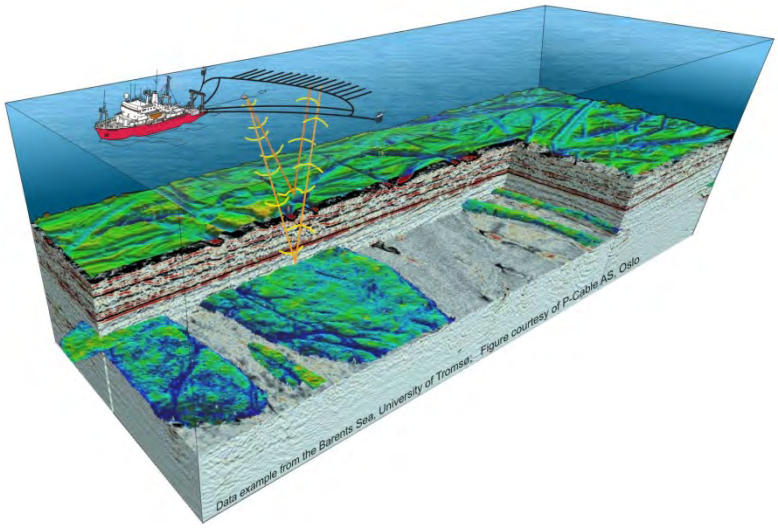

Figure 2: Conceptual sketch of the P-Cable system towing up to 24 parallel streamers with close inline spacing.

Conventional 3D seismic data acquired by the petroleum industry have yielded a wealth of new insight and greater understanding of geological structures and processes. The P-Cable technology has proven data quality, surpassing conventional 3D and equal or better than HiRes 2D. The increase in lateral resolution compared to conventional 3D seismic data is approximately one order of magnitude. This technology images the top 500-800 m of the overburden in high detail and ideally complements conventional 3D seismic data, which is the premier monitoring tool for CO_2 storage.

Other applications include drill site investigations (scientific and industrial), sea bed properties for offshore installations, shallow gas accumulations and gas hydrates, fluid migration (3D, 4D), geohazard assessments and deformation and faulting.

Typical survey design parameters

Number of streamers:	12-24
Streamer separation:	6.25 – 12.5 m
Streamer depth:	1-3 m
Source:	High-frequency (mini-GI, sparker)
Source depth:	1-3 m
Frequency bandwidth:	30-400 Hz
Production rate:	up to 20 km^2/day
Spatial resolution:	3-5 m
Temporal resolution:	down to 1 m

1.2.2 Conventional 3D seismic

2D seismic, 3D seismic and P-cable seismic all have their limitation in shallow water depths, i.e. 150 m and less. Special survey-design can improve the resolution in these cases only to some extent, whereas good processing, and especially the removal of seafloor multiples, is of crucial importance. Alternatively, seismic investigation should be complemented by sub-bottom profiling in order to fill the resolution gap around the seafloor.

Conventional 3D seismic employed by the oil and gas industry consists of an acoustic source array and a multi-channel streamer array. It has already replaced 2D surveys as a standard in the industry, but it is a large-scale operation sometimes involving several vessels with streamers and acoustic sources.

The survey design is usually optimised for reservoir depth, i.e. from 1000 m below seafloor (bsf), and therefore the receiver offset is equally large, up to 13 km. This also means that a velocity model for the subsurface is easily acquired with conventional 3D seismic acquisition. Today, many specialized survey designs are offered by different companies, involving not only streamer arrays but also ocean bottom cables (OBC) and ocean bottom nodes (OBN) as receivers. One clear advantage is the contact to the solid seafloor which enables recording of different types of acoustic waves, pressure and shear waves, which gives a better understanding of the subsurface and a clearer indication of fluid-filled compartments.

Typical survey design parameters

Number of streamers:	6 - 8
Streamer separation:	25 m
Streamer depth:	1-3 m
Streamer length:	up to 13 km
Source:	Mid-frequency (GI, airgun, airgun-array)
Source depth:	1-3 m
Frequency bandwidth:	5-100 Hz
Spatial resolution:	8-10 m
Temporal resolution:	8-10 m

2 Strategies for baseline studies

This chapter provides an overview of how to identify and characterize leakage structure in the shallow overburden of CO_2 storage sites, and provides strategies for leakage assessment, Leakage is the process by which CO_2 escapes the storage formation into overburden sediments which ultimately may end up seeping into the water column. Leakage can occur in different forms (slow seepage to catastrophic release) and along different pathways including pre-existing pathways as well bores, or self-enhanced, hydro-fractured system, mostly a vertical, focused fluid flow feature. The flow of the leaking fluids is driven by hydrological gradients and buoyancy. Most often, the latter two are governed by site characteristics and the geological setting of an area, e.g. due to compaction from tectonic stress or sedimentation.

2.1 Leakage structures and pathways

2.1.1 Seafloor features

Up to now, preferentially seismic data sets were used to characterize the overburden over potential storage reservoirs. However, fractures in the seafloor are difficult to detect with the use of conventional 3D seismic. To reveal potential seafloor leakage structures in detail, the use of an autonomous underwater vehicle (AUV) equipped with a high-resolution interferometric synthetic aperture sonar system (HISAS – commercially available) is necessary. The HISAS is capable to obtain an image resolution of up to 5 x 5 cm and can thus observe diverse detailed features at the seafloor such as fractures or pockmarks.

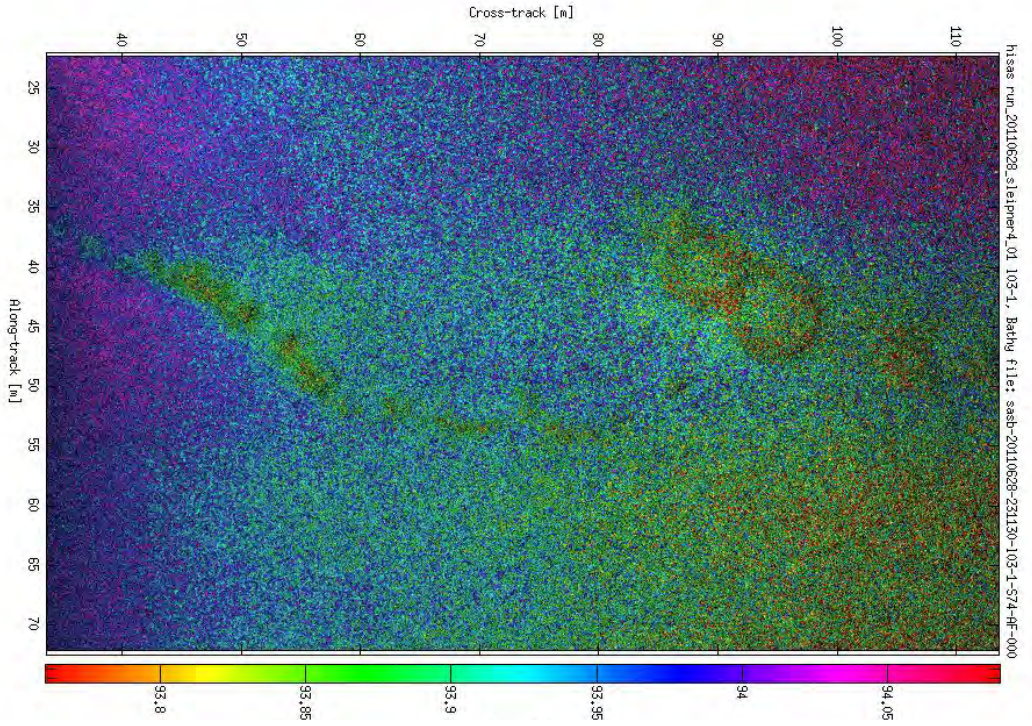

Figure 3: Example image of two ring structures. The image is a synthetic aperture sonar (SAS) reflectivity image, with colour-coded bathymetry. The diameters of the two rings are about 4-5m, and they are elevated by about 10 to 15 cm compared to the surrounding seafloor.

Fractures in the seafloor can be connected to a complex fracture network in the subsurface and give rise to active fluid or gas flow from deep geological formations into the seawater. The most obvious indicators for fluid or gas flow from a fracture are the growth of bacterial mats or bubbles rising from the seafloor. Fractures can be characterized by linear, en echelon and branching segments as well as by ring structures (Figure 3). They can be several kilometres long and vary in width and form over the distance. Due to a lack of high resolution imaging data, it remains unclear how common fractures in the seafloor are.

Pockmarks are other special features at the seafloor. Seabed fluid flow involving seepage of free methane gas and/or water with a high methane concentration in solution is found in every sea and ocean (Judd, 2003). Acoustic and seismic data can reveal seabed fluid flow indicators such as pockmarks, mud volcanoes, acoustic chimneys, pingos and authigenic carbonate build up which are related to hydrocarbon migration (Hovland and Judd, 1988). Pockmarks correspond to erosive features formed by escape of gas and/or fluids from low-permeability, fine-grained surficial sediments. Pockmarks can be subdivided into six morphological classes (Hovland et al.2002), whereby most of them fall into two classes: (1) Unit pockmarks are small depressions typically 1-10 m across and up to 0.5 m deep, and probably represent a one-time expulsion event. They are common inside and around normal pockmarks; (2) Normal pockmarks are circular to semi-circular, sometimes elongated depressions typically 10-700 m across, and from 1-45 m deep. Their cross-section varies from a basin-formed (low-angle) shape to an asymmetrical and steep-walled feature. Some are even funnel-shaped in the center.

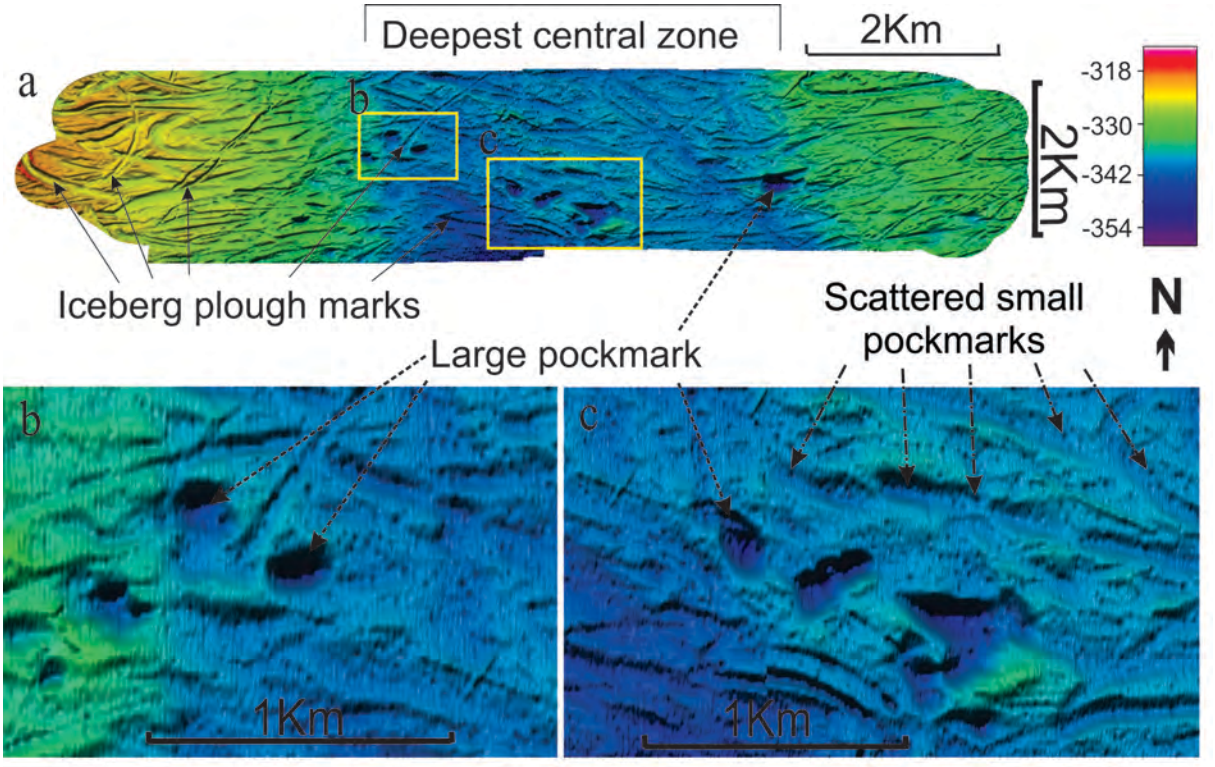

Figure 4: Pockmark characterization through Multibeam data from a) A seabed surface map from the P-Cable high resolution seismic, with data showing location and extent of Nps, Ups and ploughmarks on the seafloor and with associated cross sections 1- 5. b), and c) are zoomed in images of a) at various locations where Nps cluster.

Several large "normal" pockmarks have been observed at the study area at Snohvit (7 in number over an area of ~16Km2)(Figure 4). Also several hundreds of small "unit" pockmarks exist over the same area. All pockmarks are often found within glacial plough marks and have affected their internal structure, thus formed after them. The distribution of pockmarks is thus controlled by the orientation of the glacial plough marks. Pockmark genesis can be related to various factors but the abundance of ploughmarks at the seabed (Figure 4) suggests a mechanism related to iceberg scouring at the seafloor during ice retreat. Pockmark formation is thus not a contemporary phenomenon but a paleo-event probably linked to a deglaciation.

2.1.2 Gas accumulation – bright spots

The interpretation of 3D Seismic data is one of the most effective methods for the analysis of focused fluid flow structures and to reconstruct the evolution of fluid flow systems in marine sediments. Free gas causes significant changes of the bulk modulus of affected sediments, which manifests in seismic data as anomalous seismic amplitude patterns including increased, dimmed, bended or broken seismic reflections, and zones with vertically disrupted or chaotic amplitude distributions.

The most obvious gas-related seismic anomalies are **bright spots**, which are characterized by reflections with increased seismic amplitudes and reversed polarity (Figure 5). Bright spots can be easily identified in seismic profiles and are generally associated with free gas accumulations. They are highly variable in scale reaching from tens of meter to km in diameter. Bright spots beneath the base of a sedimentary overburden are an indicator for its good sealing properties. However, bright spots within the sedimentary overburden may suggest hydraulic connectivity between the sedimentary overburden and underlying layers. Indicators for a hydraulic connection between different layers can be a spatial correlation between bright spots in two layers or distinct vertical amplitude anomalies known as **seismic pipes** (Figure 5).

Based on seismic data, it is hard to evaluate if such pathways are active and open or inactive and plugged (by sediments or cementation). Nevertheless, mapping the bright spot distribution is an easy and fast possibility to get information about the integrity of sealing layers and to detect hydraulic connections between different stratigraphic units.

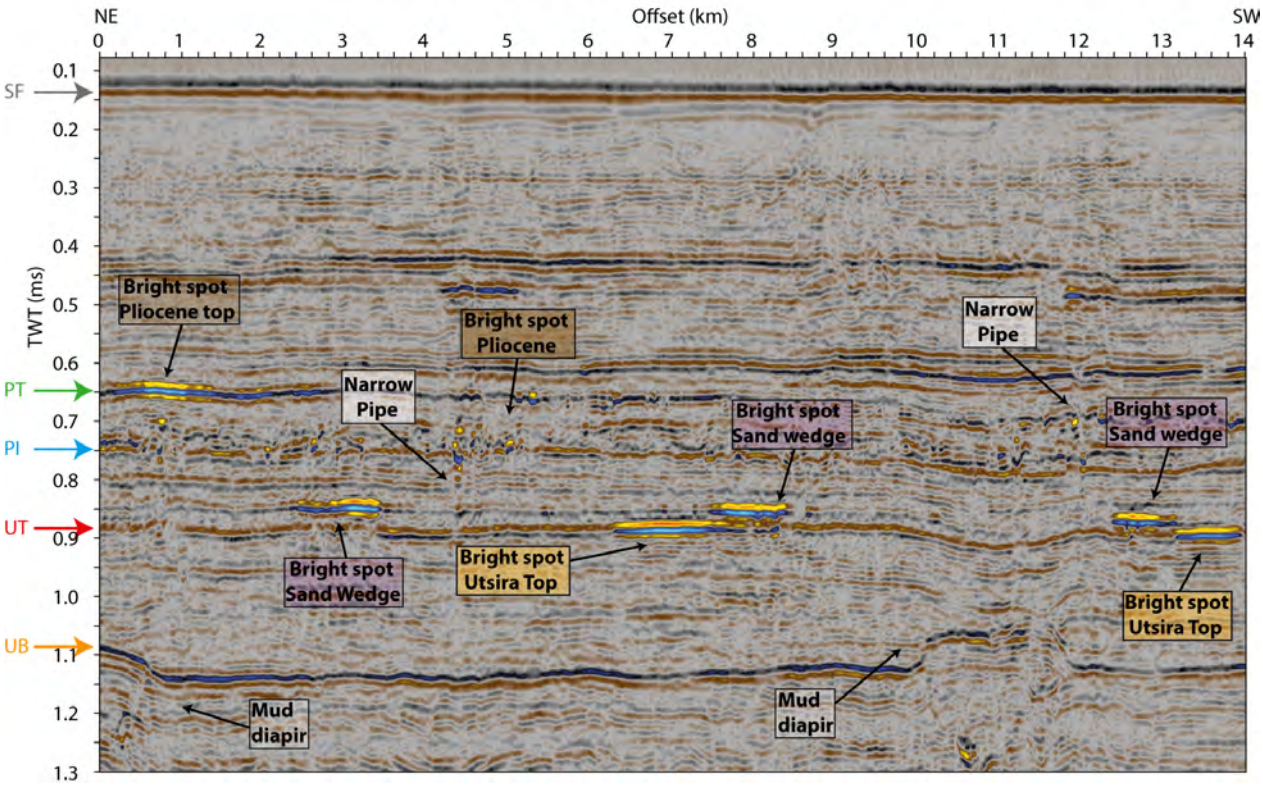

Figure 5: Bright spots in different stratigraphic levels (Karstens & Berndt (submitted))

2.1.3 Vertical seal-bypassing fluid conduits – Seismic chimneys

Seismic chimney structures are interpreted focused fluid conduits crosscutting low permeable bedrocks (Figure 6) and their scale varies from meters to hundreds of meters in length and diameter. Seismic chimneys most likely represent a continuum of geological structures including gas filled fracture networks, the remnants of single pulse blowout-like gas expulsions and zones of sediment fluidization as the result of overpressure charged fluid flow. Each process has different implication on the hydraulic properties of an affected sedimentary overburden. While fracture networks most likely represent effective fluid pathways, structures associated with blowout-like events have probably been plugged by mobilized sediments after the formation.

The analysis of chimney structures requires detailed background information and assessing the permeability of chimney structures remains highly ambiguous.

The seismic method is very sensitive for imaging seafloor parallel structures, but has however limitations in resolve vertical oriented structures. The seismic image of vertical conduits is therefore not very detailed. When interpreting seismic chimneys, it is important to rule out that the chimney itself is only a seismic artifact as the result of inadequate processing, data gaps or amplitude blanking beneath seismic anomalies. Only (repeated) 4D seismic monitoring allows a reliable evaluation of the interaction of CO_2 and a paleo fluid pathway. As a general remark, we suggest avoiding areas with a dense chimney population and complex natural fluid flow system, when choosing CO_2 storage sites.

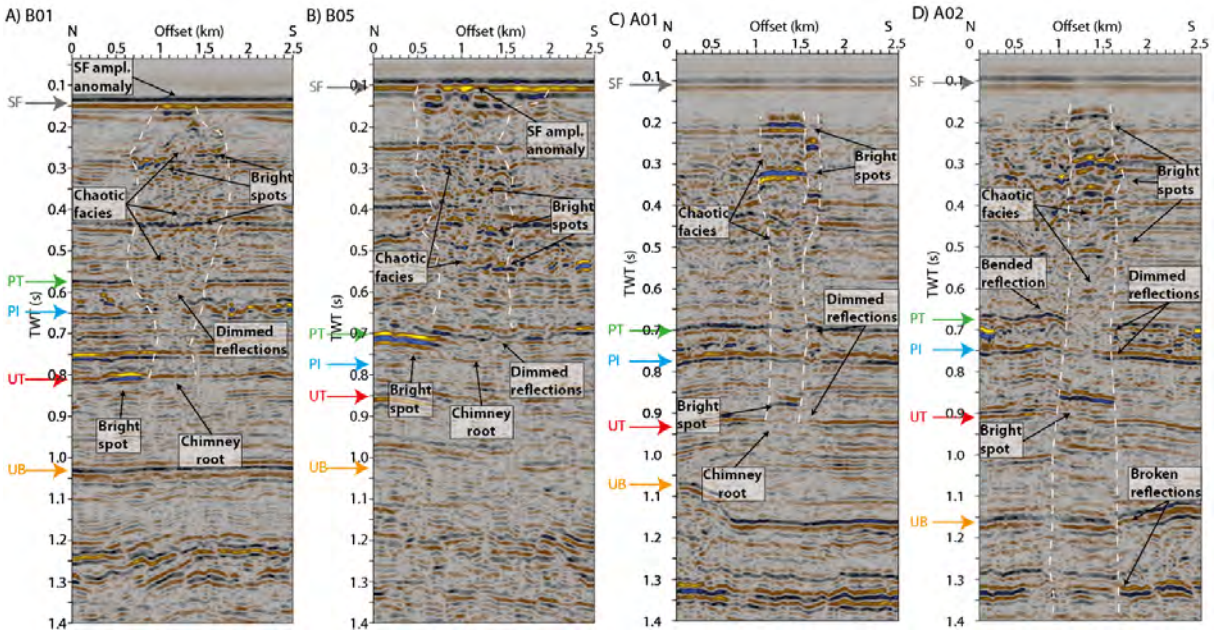

Figure 6: Seismic chimneys associated with gas-filled fracture-networks (A & B) and with rapid fluid release (C & D; Karstens & Berndt (submitted))

2.1.4 Gas hydrates

Gas hydrates are ice-like substrates consisting mainly of light hydrocarbons (mostly methane) entrapped by a rigid cage of water molecules (Sloan and Koh, 2008). Gas hydrate formation in marine sediments requires natural gas and water existing at very specific pressure and temperature conditions (Claypool and Kaplan, 1974; Kvenvolden, 1988). The stability of hydrates is also affected by the composition of gas and ionic impurities in the water (Kvenvolden, 1998; Sloan and Koh, 2008). These constraints on hydrate formation define the gas hydrate stability zone (GHSZ), the limited depth/pressure range in which gas hydrates are stable. Anomalous reflections in the seismic data, known as 'bottom simulating reflectors' (BSRs), mark the bottom of the GHSZ and are still the best indirect indicator for the presence of hydrates in marine sediments (Holbrook et al., 1996; Bünz et al., 2003; Vanneste et al., 2005) (Figure 7). This reflection is usually the result of relatively dense hydrate-bearing layer (high acoustic velocity) overlying gassy sediment (low acoustic velocity). As such, the BSR has high reflection amplitude and reversed polarity compared to the seafloor reflection. In an environment where the gas composition, water composition, sediment composition, and regional heat flow are relatively homogenous and stable, the BSR mimics the seabed topography and cuts across normal seismic reflections produced by lithological changes in the sedimentary bedding (e.g., Shipley et al., 1979). Many hydrate accumulations on continental margins worldwide are closely associated with focused fluid flow systems that provide the gas for hydrate formation (e.g., Tréhu et al., 2004; Hornbach et al., 2008; Hustoft et al., 2009a).

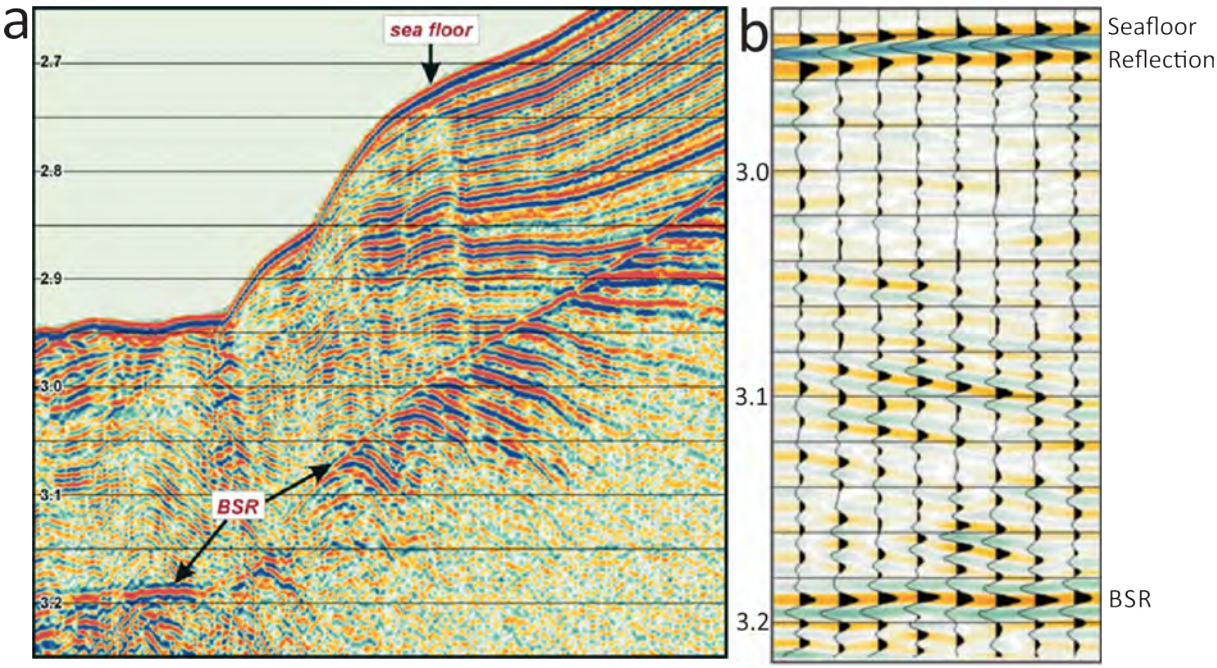

Figure 7: a) Typical seismic expression of a BSR (example from western Svalbard margin). b) Wiggle trace display illustrating high-amplitude of the BSR and its reverse polarity with respect to the seafloor. (Figure modified from Vanneste et al. (2005)).

3D seismic data from the Snøhvit ares indicates but does not conclusively document the presence of gas hydrates. Some short, segmented high-amplitude anomalies in the shallow overburden could also be just related to gas accumulations of large chimney structures.

2.1.5 Faults

During faulting granular material causes cataclasis and the porosity changes. A measurement of porosity values in the subsurface, via drilling and logs, and subsequent comparison of the values over an area would thus indicate the possible location of faults.

We can detect leakage structures such as past or present leaking faults via high amplitude anomalies (bright spots) that are found either above them in shallower strata (Figure 8B and 8D) or where the faults terminate (Figure 8E and 8F). Further indication for fluid migration in faults is the presence of acoustic masking in a narrow zone along the fault planes. Other evidence of fluid migration includes high amplitude anomalies along the faults and structure fitting high amplitude anomalies within the fault hanging walls.

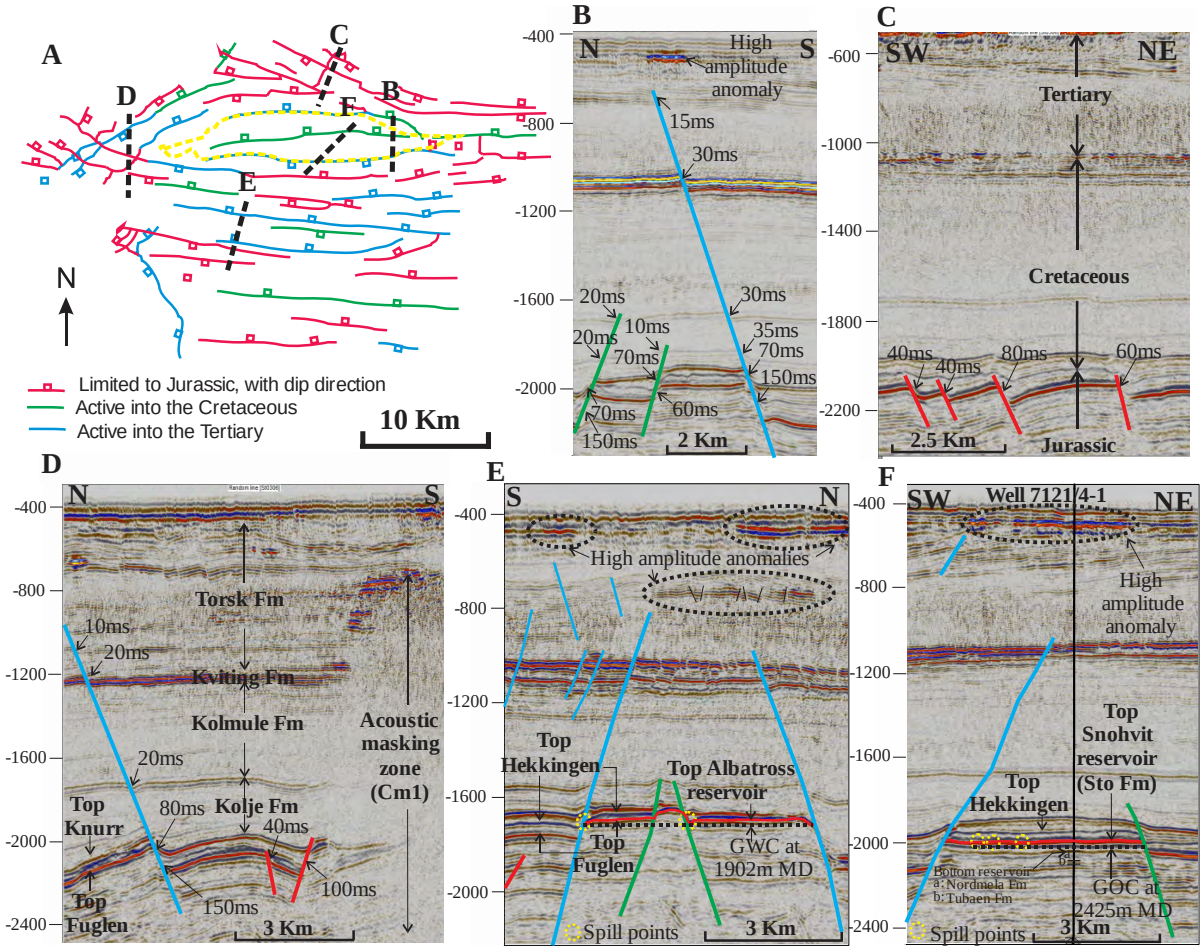

Figure 8: A) Pattern of large scale faulting in the area, Cross sections through B) Cretaceous and Tertiary faults, C) Jurassic faults, D) various faults and CM1. Association of faults and spill points at E) Albatross and F) Snohvit reservoirs.

The critical controls on leakage of CO_2 through faults thus include along and up fault permeability, CO_2 injection induced pressures leading to fault reactivation or fracturing and the presence of pathways connecting the fault through the overburden to the surface (Figure 8). Major deep seated faults may have thus functioned or still function today as fluid flow pathways and the upward migration of fluids leads to accumulation in the shallow subsurface (Figure 8B). Fluid migration through faults, taking place through micro-fracturing or molecular diffusion, allows such faults to act as valves for the transport of fluids along the fault plane.

Once we have detected a potential fault plane in the seismic we can further assess whether it's a sealing or a leaking structure by looking at the lithology and its characteristics on either side of the assumed fault plane. Fault plane profiles thus allow us to infer the sealing behavior of faults. Seal behavior is further inferred from hydrocarbon contacts and pressure data as well as several types of fault dependent leak points and log measurements (e.g. gamma ray logs) (Figure 9) For example in a cross sealing juxtaposition, we could have 2 different sands on either side of the fault plane; the hydrocarbon bearing sand being placed against a water-wet sand. In a cross leaking juxtaposition, we would expect for the sand juxtaposition to have either a common GWC (gas-water contact) or both a common GWC and GOC (gas-oil contact), thus providing evidence

of cross leakage at both sand/sand juxtapositions. One leaks gas; the other leaks both oil and gas (Figure 9).

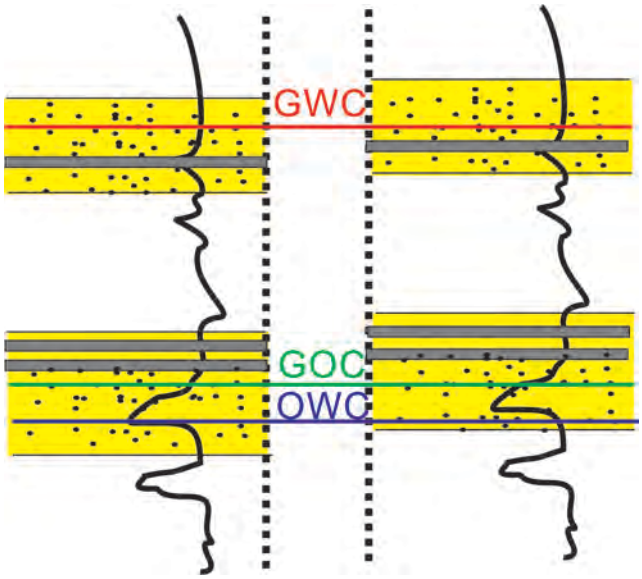

Figure 9: Seal behavior in a cross sealing juxtaposition

Fault seal analysis involves uncertainties and risk. Assessing the sealing or leaking capacity of a fault involves having a good understanding of the stratigraphy and fault displacement and structure in the study area. Changes in stratigraphy such as the presence of a thin thief sand can dramatically affect seal risk. Variations in stratigraphy and displacement will change the Smear Gauge Ratio (SGR) and juxtaposition relationships along the fault. The fault mapping procedure may also involve varying degrees of uncertainty. The stratigraphy may also vary through a range of net/gross, sand thickness, and shale thickness.

To reduce uncertainty we should focus on obtaining a range of probable values and applying a Monte Carlo analysis approach. Given the above uncertainties, it's important to recognize the really critical elements during interpretation. Interpreting a certain end of a specific fault or focusing on the stratigraphic variation within a specific systems tract or determine the probability of a specific sand/sand juxtaposition may be required.

2.1.6 Other stratigraphic structures promoting fluid flow

Paleo-channels

To document the shallow subsurface expression of a seafloor fracture system as well as to determine the relevance of the fracture for seal integrity, a combination of high resolution and conventional 3D seismic data sets as well as sub bottom profiling is the recommended strategy.

In an example from the North Sea (Hugin Fracture), a combination of sub-bottom profiling and conventional 3D seismic allowed for in depth investigation of a seafloor fracture over several scales, which would not have been possible with only conventional 3D seismic. The sub-bottom profiles revealed a vertical disturbance from the seafloor down to 50 m with a vertical resolution of tens of centimetres. Projected on the 3D seismic data the vertical disturbance aligned very well with a buried channel structure, but the fracture itself is below 3D data resolution. Further interpretation of the 3D seismic volume revealed a large number of buried channels with indications of fractures in-between some of them. By combining sub-bottom profiler data and 3D seismic, a complex network of fractures and channels could be identified

and tied to the seafloor fracture, going all the way down to the Pliocene (see Figure 10). Whether this network actually is open to fluid flow and what rates of CO_2 leakage it would allow for cannot be determined from 3D seismic interpretation alone. The next steps in doing that would be, drilling of shallow wells in the most interesting channels, to validate the seismic interpretation, and modelling the discovered geometry with different values for parameters relevant for fluid flow, such as porosity and permeability for the channel sediments and pressure increase in CO_2 storage reservoir due to CO_2 injection.

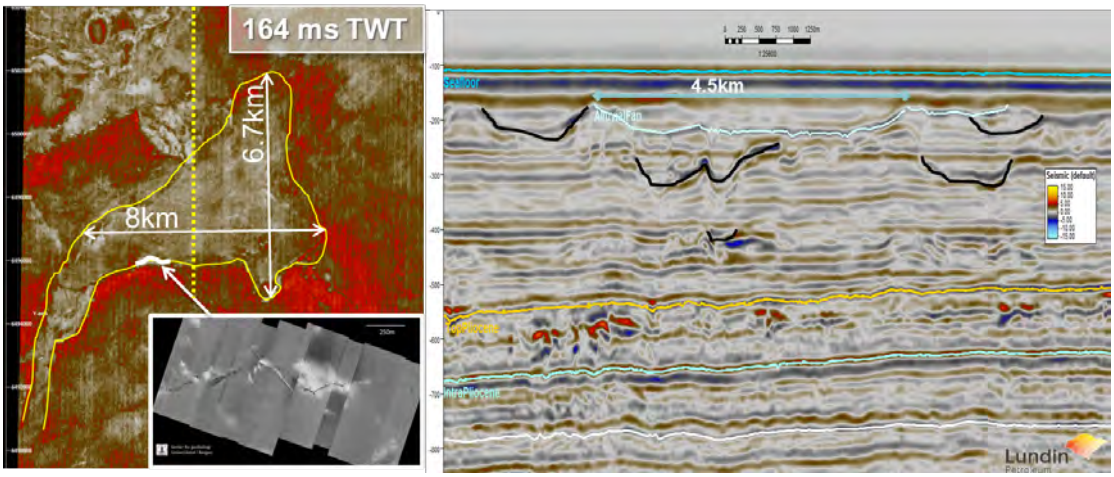

Figure 10: example from 3D seismic interpretation at the Hugin Fracture. Left: map view from 70 m below seafloor with the highlighted outline of the channel just below the fracture on the seafloor. Right: depth section of the seismic data with highlighted channels in different depths.

Clinoforms and lateral migration

Evidence of subsurface lateral flow may be indicated by stacked, segmented high-amplitude anomalies along dipping strata. In the Barents Sea, this is a widespread pattern of fluid migration due to the differential uplift and tilting subsequent to multiple glaciations as shown in Figure 11. Gas migrates up the dipping strata up to where an unconformity truncates the sedimentary bedding. Here gas accumulates leading to shallow gas occurrences. Such anomalies are best imaged in 3D seismic data which is able to reveal the extent and nature of such gas accumulations.

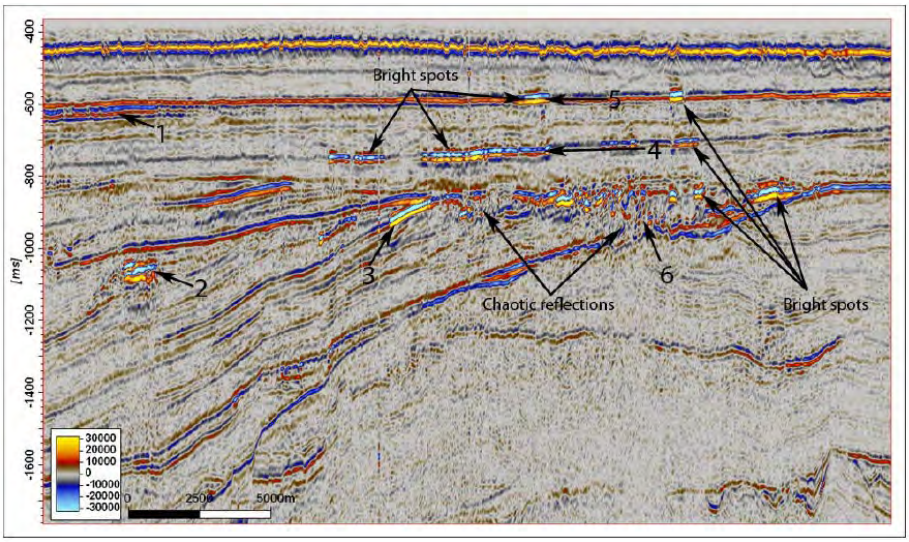

Figure 11: Seismic example from the Barents Sea showing gas migrating updip along the sedimentary strata.

In the Snøhvit area, the presence of a clinoform system in the Torsk formation has been mapped, dipping at an angle of about 10-20˚, under the upper regional unconformity (Figure 12). The stratigraphic dip related to the clinoforms in the upper Torsk formation shows indications of controlling fluid movement. There is strong evidence that clinoforms act as fluid flow pathways and determine the location of pockmarks at the seabed e.g. see pockmarks forming at the same distance from the edge of clinoforms and coincidence in orientation of clinoform edges and pockmark alignment. Some normal pockmarks seem to form at roughly the same distance i.e. a few hundred meters from the edge of clinoforms (200-400m).

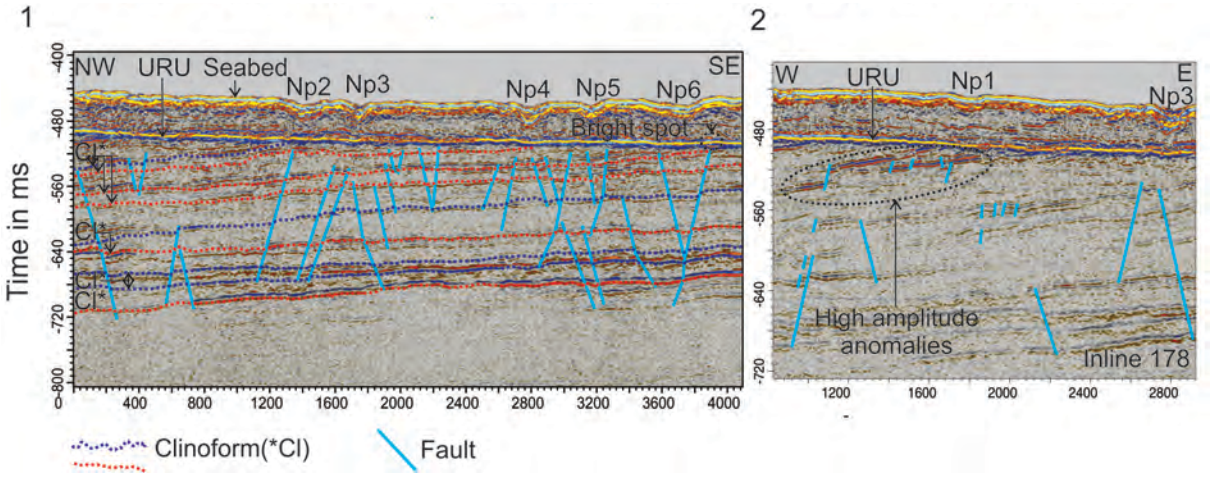

Figure 12: Seismic example of P-Cable high-resolution 3D seismic data illustrating the shallow overburden stratigraphy in the Snøhvit area with 1) underlying faulting and bright spot, and 2) shallow and deep faults with associated high amplitude anomalies.

2.2 Leakage assessment

Leakage assessment is a process by which an understanding of potential leakage scenarios is developed. It is a purely hypothetical process and does by no means imply that storage site integrity is compromised by the sheer presence of leakage structures.

This leakage assessment process includes four key components:

- the ability to detect a potential leakage pathway;
- the ability to detect small fractions of leaking gas;
- the identification of potential leakage scenarios;
- the qualitative assessment of the likelihood of leakage considering site characteristics and the geological setting.

The analysis of subsurface data may reveal a number of fluid-flow features, as for example gas chimneys, pipes, shallow gas accumulations, leaking faults, fractures along the seafloor as well as gas hydrates. Each of these structures or set of structures must be evaluated with respect to their occurrence, distribution, origin and as a means for providing a potential pathway for CO_2 if it would leak out of the storage formation. On the basis of this evaluation and the assumptions that paleo fluid-flow structures may be reactivated by CO_2 injection and that the sedimentary overburden of the storage formation may breach, a number of potential leakage scenarios may be formulated for offshore CO_2 storage sites. The leakage scenarios largely include leakage along a chimney (blow-out structure) or along a fault but are adapted to the specific geological background at each storage site and hence, depending on its exact subsurface location and context may yield a complex migration pathway for CO_2 from the storage formation to the seafloor. Leakage scenarios can be implemented into fluid flow simulations that cover the whole overburden and thus support the leakage assessment and provide rough estimates on leakage rates and duration, though, with yet large uncertainties.

2.2.1 Leakage scenarios

We advise to develop leakage scenarios based on the analysis of the data sets collected for the baseline study. In addition, literature data and experiences from comparable projects should be taken into account. The general approach for developing leakage scenarios is the following:

1. Obtain baseline data and examine literature and experience from past events.
2. Check baseline data for special features in the seafloor and sub-seafloor.
3. Develop potential leakage scenarios.

The most likely leakage scenarios developed within the ECO$_2$-project for CCS storage sites are the following:

1. Through pre-existing fluid flow systems
    a. Blowout
    b. CO_2 escape through chimneys
    c. Formation water discharge through chimneys
2. Abandoned wells
3. Through interconnected pathways involving fluvial channels

1a. Blowout
The first potential scenario is the creation of a CO_2 blow out. Such a process may be comparable to the Tordis incident in 2008. The Tordis incident occurred as the result of waste water injection in a thin sand formation. After a period of 5.5 months of injection accompanied with a constant formation pressure increase, the 900 m thick overburden fractured and water discharged in a blowout process for 16 to 77 days (Løseth et al., 2011). It enabled a build-up of high overpressures necessary to hydrofracture the impermeable seal and thereby creating a blowout.

1b and c. Chimneys
Seismic chimneys rooting as deep or even deeper than the storage formation are potential escape pathways for CO_2 or formation water. Such features are likely high permeable conduits, even tough the permeability of seismic chimneys is not well constrained yet and may even vary with the age of such structures due to self-sealing cementation processes. However, especially in low permeable rocks such as shales, the influence of fracture induced permeability is high and relates to the spacing, length and orientation of the fractures (Guiterrez et al., 2000). Fractures change the permeability of sediments permanently because even fractures that are defined as closed due to changes in the stress regime continue to have much higher permeability values in their matrix (Guiterrez et al., 2000).

2. Abandoned wells
Numerous abandoned wells drive through geological formations in areas of oil and gas exploration and thus break through the natural sealing layers. This results in possible pathways for fluid and volatiles to migrate from deep geological formations up to the seafloor. Confirmed leakage of biogenic CH_4 at the abandoned wells in the North Sea clearly demonstrate the possibility of gases rising from or along abandoned wells through the sediments into the water column (this project).

3. Interconnected pathways
If seismic data of the target area reveal channels of fluvial or glacifluvial origin, as found in the area of the Hugin Fracture, then a connection between these channels and tunnels could be a potential leakage pathway. Previous studies show that in the North Sea, a complex pattern of filled tunnel valleys have been formed sub-glacially by melt water during deglaciation of the last few full-glacial periods (Huuse & Lykke- Andersen 2000; Praeg 2003; Fichler et al., 2005; Lonergan et al., 2006). The tunnels may reach several tens of kilometers in length, can be several hundred meters deep and up to five km wide, and the sediment infill of the tunnels is mainly silt and sand (Kristensen et al., 2008). Such channels are accordingly potential pathways for lateral fluid flow.

3 Strategies for monitoring the shallow overburden

3.1 Seafloor and shallow overburden

Strategy for baseline studies and monitoring of the seafloor above of a potential CCS storage site:

1. Use hydroacoustic data to see if bubbles are leaking from the seafloor.
2. Use bathymetry to get information about the seafloor topography and search it for special features.

3. Survey the target area with an AUV equipped with a HISAS to get detailed information of the seafloor features. Special features, as for example the Hugin Fracture, are often not visible in other data sets than HISAS operations.
4. Obtain bathymetric, photographic and chemical sensor data collected by an AUV to check if special features, like fractures, show active fluid flow.
5. Use seismic data sets to get information on the sub-seafloor structures to check the integrity of the seal formation and if there are channels, pipes, fractures or faults visible. Check if the observed features are connected with each other and provide an escape pathway for gas or fluid.
6. Based on the collected information, evaluate if a present feature at the seafloor is
    a. Natural
    b. Common in the area
    c. a risk for a CCS site.

If active fluid flow at the seafloor is observed, distinct sampling of the fluid/gas with gastight samplers is strongly suggested. Subsequent analysis of the chemical and isotopic composition of the leaking gas/fluid will provide information about the quantity of leakage as well as its source.

3.2 Overburden between sedimentary overburden and seafloor

The monitoring of the overburden (between the sedimentary overburden and the seafloor) to detect the leakage of CO_2 from a storage reservoir is best undertaken with time-lapse 3D seismic data.
The substitution of brine by CO_2 causes changes in the reflectivity of the subsurface which can be imaged using 3D seismic data. Analysing the difference signal between time-lapse vintages offers the best opportunity to determine leakage. Robust spatial and volumetric coverage is provided by time-lapse seismic data with common bin spacing of 12.5 m giving a detection capability at high resolution.

Leaking CO_2 will be distributed in two ways in the shallow overburden: (1) in layers, which should produce observable seismic reflections; and (2) as diffuse chimneys of CO_2, which will generate time-shifts on deeper, underlying reflections.

As such, leakage detection requires a reproducible technique to identify reflections generated as a consequence of leaking CO_2, within a noisy dataset. This methodology must utilise the brightness and spatial extent of changes observed in the time-lapse difference data (Figure 13). This difference signal contains random noise components alongside systematic repeatability noise where the signal from the geology has been poorly matched between vintages. Consequently, parts of the overburden are 'quiet' with low repeatability noise and high detection capability, whereas other parts have higher repeatability noise and exhibit poorer detection capability. Therefore the detectability will vary as a function of depth.

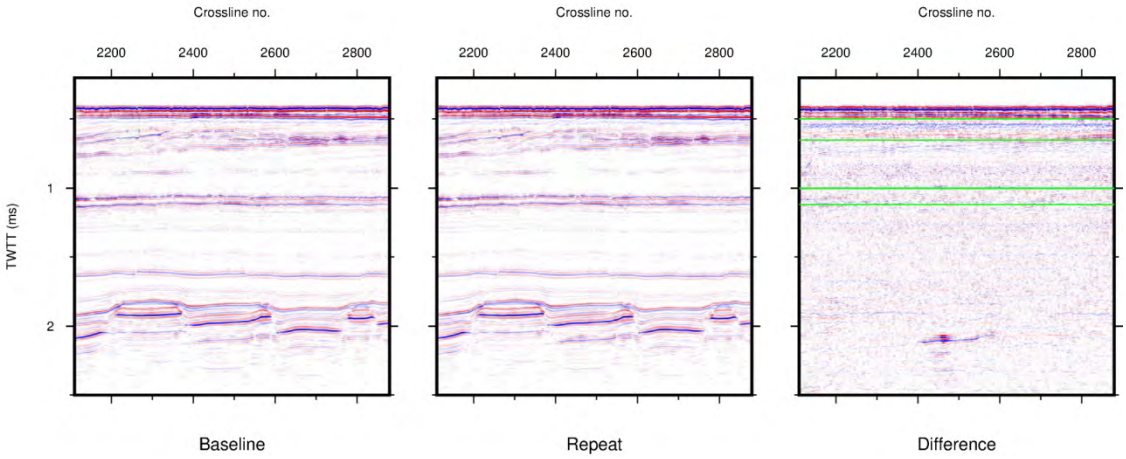

Figure 13: Time-lapse seismic data from Snohvit offshore storage operation in the Barents Sea. The response caused by CO_2 injection into Tubaen reservoir is clear (at 2.1 s) and differing levels of noise in overburden are seen. Green lines highlight locations of time-slices used in Figure 14.

Analysis of time-slices (Figure 14) within the overburden offers a statistical, and automated, methodology to determine leakage and leakage thresholds. The discrete wavelet transform can then be utilised to define the noise components over different spatial scales for each of the time-slices. It is then possible to define noise thresholds where anything distinguishable from the background noise could be a signal from leaking CO_2. Detection depends on the area of a CO_2 layer, and its layer thickness, which determines the seismic amplitude. Utilising this method the minimum size of accumulation that can be detected can be defined.

As part of ECO$_2$, a set of tests were carried out to examine the detectability of synthetic CO_2 accumulations on real seismic time-slices by adding reflections of known size, circular geometry and of uniform amplitude. The synthetic accumulations were added to the time-slices at random locations. By running the simulation numerous many thousands of times the statistical likelihood of detection as a function of amplitude and area can be produced. Figure 3 displays the probabilities of detection and it is apparent, in all cases, this increases with area and reflectivity amplitude.

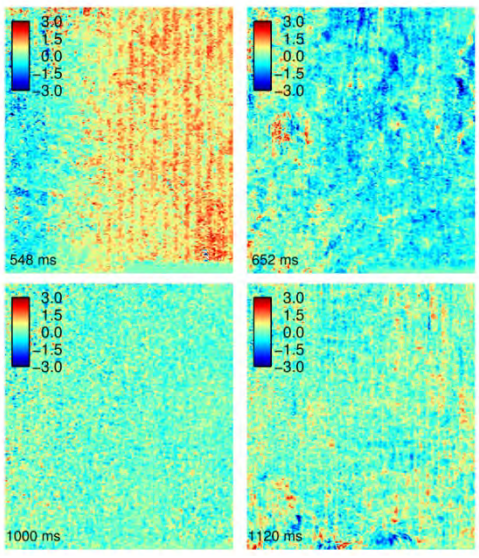

Figure 14: Differing noise characteristics on time-slices (at 548 ms, 652 ms, 1000 ms and 1120 ms) from seismic difference data cube over Snohvit offshore storage operation.

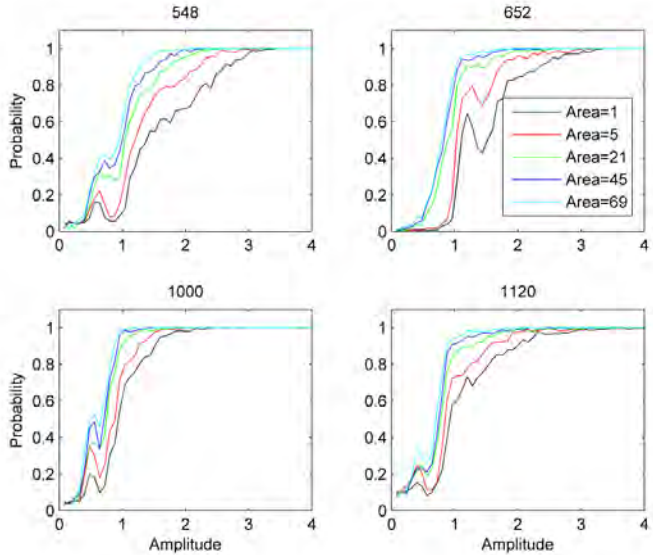

Figure 15: Probability of detecting circular synthetic CO_2 accumulations against reflection amplitude (for 548 ms, 652 ms, 1000 ms and 1120 ms time-slices). The area is defined in terms of number of seismic trace bins (each 12.5 x 12.5 m).

It is notable that detectability decreases progressively in the shallow section towards the seabed (Figure 15). This is because the low folds of stack and more variable ray-path geometries result in poorer time-lapse repeatability. In order to maintain detection capability in the shallow section it might be desirable to overlap the conventional 3D seismics with a shallower-focussed 3D seismic technique such as p-cable. The repeatability of p-cable data at Snohvit is currently being tested to see if this is a viable option.

In order to derive true CO_2 mass detection thresholds it is necessary to transform the amplitude detectability statistics into CO_2layer thicknesses and saturations using rock physics and a CO_2 equation-of-state. This has been carried out for the time-lapse datasets at Sleipner (Chadwick et al. 2014), which indicate that under favourable conditions, amounts of gaseous CO_2 as small as 300 tonnes might be detectable at shallow depths (< 500 m).

4 Modeling strategies to support leakage assessment

In order to assess the environmental impact of potential CO_2 leakage at a proposed CCS site, it is necessary to perform fluid flow simulations that consider existing natural or hypothetical fluid pathways in the sedimentary overburden of a storage reservoir. Such simulations can help to understand the long-term evolution of migrating CO_2 and can be used as the base of monitoring strategies.

Modeling of the physical and chemical processes occurring in nature is a demanding task and model development requires a multi-stage approach to describe the system (Figure 16). In the following, the five stages are described in more detailed and put into the context of ECO$_2$ project.

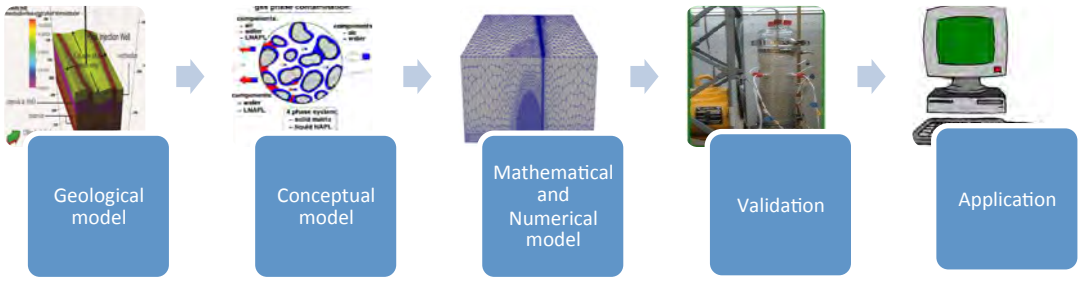

Figure 16: Model Development Process

4.1 Geological Model

Interpretation of the geological structures is the first step in modeling leakage of CO_2 from the storage site. Modeling complex geological settings is a demanding task, which highly depends on the available data, interpretation techniques and also on the spatial scale of the model. One of the major difficulties in assessing potential leakage scenarios from fluid flow simulation are the uncertainties of the model. These uncertainties have to be kept in mind, when developing and parameterizing geological models and evaluating simulation results. A geological model should be as simple as possible and as detailed as necessary and has to offer a possibility to update the geological parameters to match them with field observation. Figure 17 shows the process of building geological models.

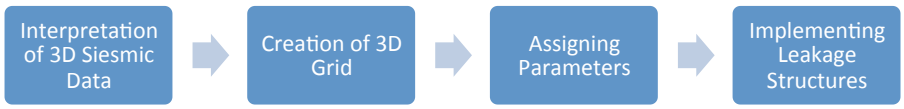

Figure 17: Geological model building process

Two examples for such models covering the CO_2 storage sites of Snohvit and Sleipner were developed for the ECO2 project. The development of geological models for Snohvit were based on the interpretation of the 3D conventional seismic data (ST0306) provided by Statoil. The 3D seismic interpretation software Petrel by Schlumberger was used to analyze the seismic data, integrate well-log information and build the geological models as an input for the fluid flow simulations. Because of the complexity of the local geology, we implemented three different geological models, where each only considers one type of migration pathway: i) Fault model ii) Realistic gas chimney model iii) Generic gas chimney model. To account for the uncertainty of the hydraulic parameters of the fluid pathways and the bedrock, these models were further divided into three different realizations with low, medium and high porosity and permeability values.

For the Sleipner CCS project we developed three different geological models, which include or exclude specific stratigraphic units depending on the scientific objectives. The first model does not include the complete overburden or leakage structures and was used to define the permeability field by matching the modeled CO_2 plume shape with the real shape derived from time-lapse seismic data. The other two models include the complete overburden and leakage structures. While one model considered two different kinds of chimney structures (Type A and Type C), the other included only Type-A-chimneys. Both realizations had the same permeability field for the storage formation, which was derived from the initial plume shape simulations.

4.2 Conceptual Model

When CO_2 is injected in a saline aquifer, it can occur as a separate phase, be dissolved in the formation brine or chemically react with other phases. Considering all of the processes at once, is not feasible for large model domains due to computational limitations. For example the large-scale fluid simulations for Snohvit and Sleipner are too coarsely resolved to consider chemical reactions of CO_2. Therefore, it is important to evaluate the model requirements based on the scientific questions prior to running simulations. For the Snohvit and Sleipner field, we considered simple conceptual realizations, which neglected the dissolution of CO_2 in the formation brine, as well as significantly more time consuming simulations including the CO_2 dissolution.

CO_2 injection into a saline aquifer will cause pressure buildup in the storage formation, which will in turn change the state of stress in a reservoir-seal system. As a result of poro-mechanical and thermally induced stress changes the sealing capacity of pre-existing faults may be changed and exceeded, or faults may be re-activated, affecting the CO_2 migration. Poro-mechanical and thermal effects associated with CO_2 injection may also cause fracturing of the sedimentary overburden, thus creating of new leakage pathways for CO_2 migration towards the seabed. It is therefore important to consider geomechanical processes when developing simulation models for a fault leakage scenario, which is done for the Snohvit field case.

4.3 Mathematical and Numerical Model

We used the DuMu^x [Flemisch et al., 2011] open source porous media simulator, which is able to choose different models and numerical techniques to solve the multiphase system. The first step of the numerical modeling is to generate a grid for the simulation. As mentioned before, the grid size and resolution has to be carefully considered to fit modeling requirements as well as computational resources. These requirements resulted in a model resolution of 50 m x 50 m for Sleipner. Once the grid is defined, the next steps include assigning of boundary condition, initial values, fluid properties and reservoir parameters. Initial simulation runs are usually realized using available literature values to verify the results with available experiment data and to evaluate and iteratively update the conceptual model.

For geomechanical simulations we used the finite element package DIANA [TNO Diana, 2014. DIANA: *Finite element program and User Documentation*, version 9.5 (www.tnodiana.com).], which offers a wide range of constitutive models for geo-materials and frictional behavior of faults. The meshes for geomechanical numerical models have resolution similar to that used in the DuMu flow simulation grids. Common structural boundary conditions and initial loading conditions are applied, based on the available Snohvit field data. Transient pore pressures from flow simulations are used as input loads to the geomechanical simulator to assess the geomechanical stress changes and the associated deformation, including the hydro-mechanical impact on faults.

4.4 Validation

In case of ongoing projects, simulation models can be validated with field observation. A good example is Sleipner, where information about the CO_2 distribution in the subsurface can be derived from the time-lapse 3D seismic. By changing hydraulic parameters and comparing simulation results with the seismic data, we were able to choose the most suitable parameterization for our model. Figure 11 shows the plume shape for different years for the best matching model.

4.5 Application

Once the model is developed and validated, simulations may help to predict the CO_2 plume evolution and the potential interaction with fluid pathways in the overburden of a CO_2 storage reservoir. It also helps to estimate the amount of possible leakage from a CCS site and to develop monitoring strategies.

As an example for Snohvit, after developing the model, a sensitivity analysis of different parameters such as structure thickness, structure permeability and background permeability were performed keeping in mind to get a useful insight into parameters for future projects. By performing such an analysis, we could thus determine whether we need to know the permeability of the structure for example, whether it is necessary to drill into it and how important is a certain parameter for the CO_2 migration assessment. It also gives an insight into how the CO_2 will distribute in the formation for different realizations and which migration pathway it will take to reach the surface (see Figure 18).

Geomechanical simulations focused on predicting induced stress changes due to pressure buildup in the Shovhit storage reservoir. The impact of injection-induced stress changes on the hydro-mechanical behavior of faults, which may serve as conduits for CO_2 migration from the reservoir to the seabed, was studied in a hypothetical fault-leakage scenario. Limited sensitivity analysis on the effects of fault properties on their hydro-mechanical behavior was performed.

In case of the Sleipner field simulation we were able to validate the model with CO_2 plume shape with 3D seismic data. It helped us to estimate the effect of hypothetical continuous injection for 200 years and to identify which migration structures are more critical (see Figure 19). We were also able to quantify the probable leakage from these structures.

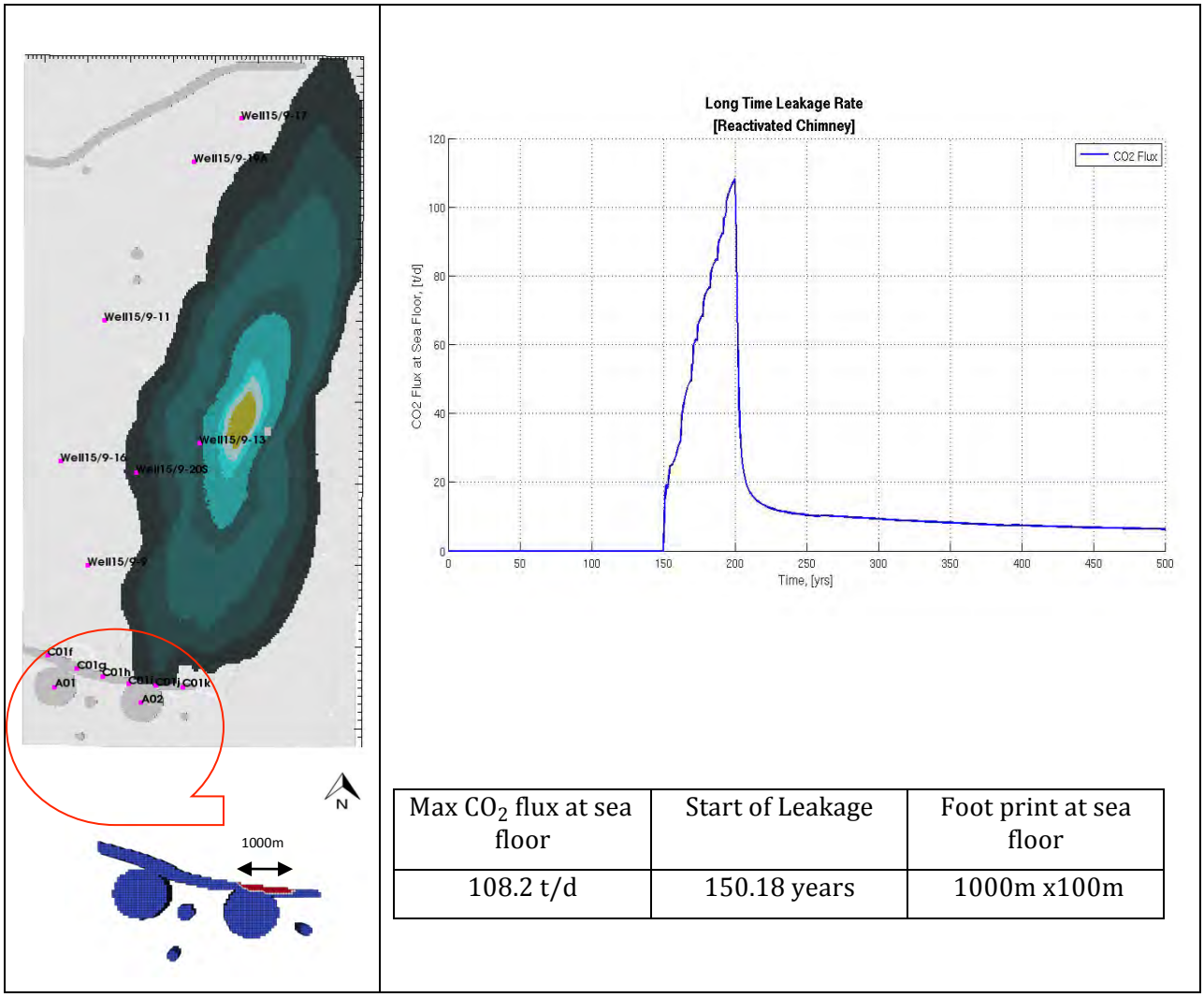

Max CO_2 flux at sea floor	Start of Leakage	Foot print at sea floor
108.2 t/d	150.18 years	1000m x100m

Figure 18: CO_2 Plume shape after 6,9,13,30,50,100,150 and 200 yr of start of injection [1Mt/yr injection for 200 yr] and Leakage rate at the surface for model considering Type A and Type C chimney.

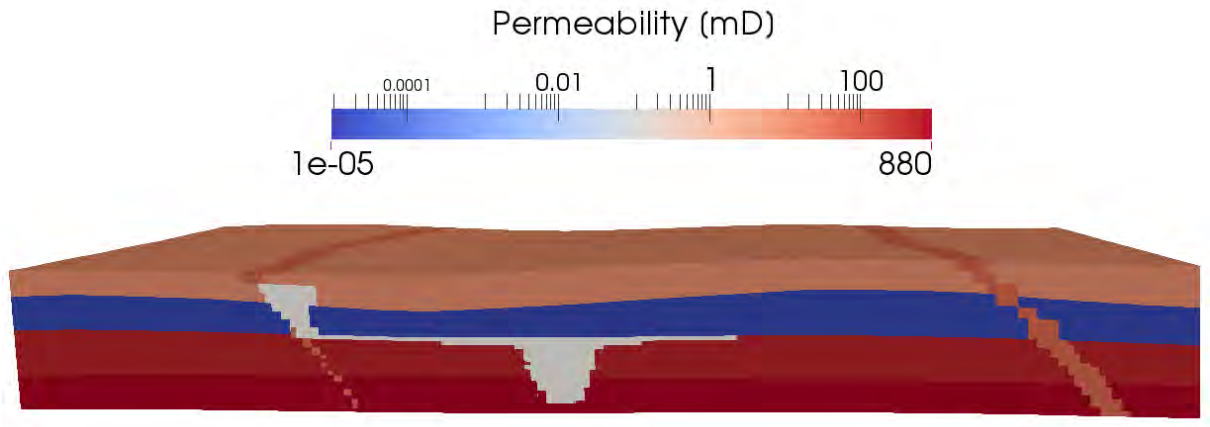

Figure 19: CO_2 plume distribution after 50 years within the low background permeability field (Fault thickness: 50m, fault permeability 50mD).

4.6 HW-Lattice-Boltzmann Methode

HW-Lattice-Boltzmann Method (LBM) model is a Non-Darcy's law model, which was developed to predict the mechanism of CO_2 plume development in a given structures of sediments or sedimentary overburden. The CO_2 leakage from deep reservoirs (liquid) and shallow sediments (gas) can be descripted by a set of transportation equations of distribution function, $f_i(x,t)$, of fluid k,

$$f_i^k(\mathbf{x}+\Delta t, t+1) - f_i^k(\mathbf{x},t) = -\left[f_i^k(\mathbf{x},t) - f_i^{k,eq}(\mathbf{x},t)\right]/\tau^k \quad (1)$$

The local equilibrium distribution function, $f_i^{k,eq}$, is obtained from Chapman-Enskog expansion of Maxwellian to the second order to describe the fluid interactions. The macroscopic density and velocity of the fluids are then calculated by

$$\rho^k = \sum_i f_i^k \qquad \rho^k u^k = \sum_i f_i^k \cdot e_i \quad (2)$$

The interfacial interactions and other forces are modelled by correction of equilibrium velocity $\rho^k u^{k,eq} = \rho^k u^k + \tau^k \cdot F^k$ and the forces, Fk, modelled in the current HW-LBM are the buoyancy, interfacial interactions, and dissolution.

A multi-range phase/fluid interaction was developed to simulate the large density ratio of water and CO_2 ($1\sim10^3$) [Khajepor et al. under review] and a new dissolution LB model was developed to predict CO_2 dissolution in brine [Wie and Chen, to be submitted]. Model is calibrated by Lab experiment [Someya et al. 2005] on CO_2 dissolution and free rising, as shown in Figure 20. HW-LBM was applied to predict CO_2 dispersion and dissolution in porous channels with sizes (M=Dc/Lc, where Dc is the size of CO_2 and Lc is the size of porous channel at dimensionless time $t^*= t/t_d= 6$, which is the time scale ratio of dispersion to diffusion) and angles (θ=90^o, 60^o, 30^o, 10^o), as shown in Figure 21. It is found that the vertical dispersion rate can be reduced about 40% when M increase from 0.3 to 1.0. Meanwhile the dissolution rate varies within 2-3%. When M<0.5, the CO_2 may break up into two or more parts as dispersion. When the channel inclines, CO_2 then disperses 30% and 50% slower at M=0.3 and M=1.0, respectively, when θ changes from 90^o to 10^o and dissolves 60% and 30% slower. The geomation structure of inclines effects more on the CO_2 dissolution.

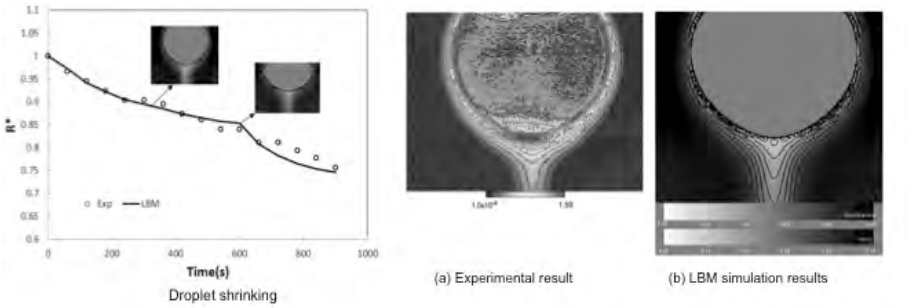

Figure 20: HW-LBM Model calibration by simulation of Lab exp of CO_2 droplet dissolution.

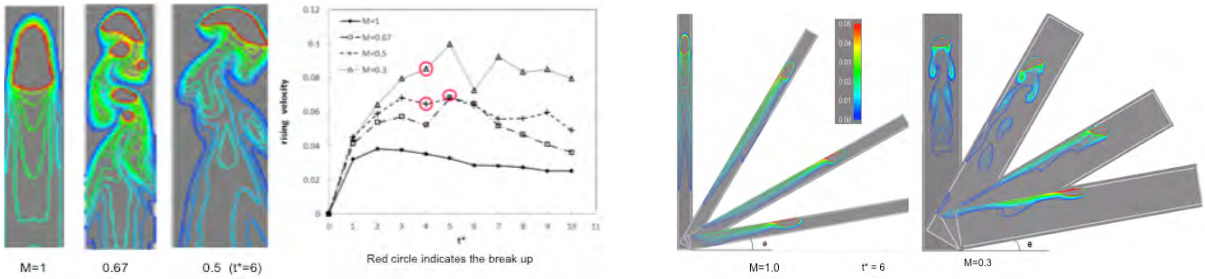

Figure 21: CO_2 dispersion and dissolution in porous channels with variant sizes (left) and angle (right)

The model is applied to simulate the CO_2 dispersion through a deep porous formation and shallow sediments with porosity of 0.35, as shown in Figure 22. The boundary condition of top-bottom of the computation domain is Δp= 0.1 and horizontal is periodic. It is found from the model simulations that the mechanism of CO_2 leakage in the deep formation where CO_2 is liquid with density ratio of 0.1 is significantly different with that in the shallow sediment where CO_2 is gas with density ratio of 2.0×10^{-3}. The large buoyancy of gas CO_2 drives it penetrate fast through the sediments to form a 'chimney plume', meanwhile, the CO_2 in deep formation can disperse horizontally and saturate the formation.

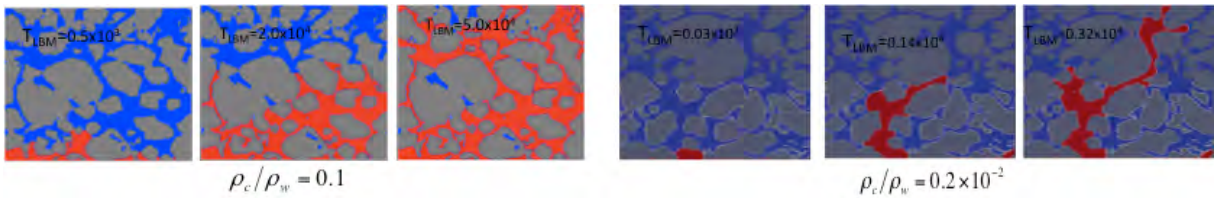

Figure 22: CO_2 (red) plumes developed in the deep formation (left 3 images) and shallow sediments (right 3 images).

Acknowledgement

The research leading to these results has received funding from the European Community´s Seventh Framework Programm (FP7/2007-2013) under grant agreement no 265847.

References

Brandvoll, Ø., O. Regnault, I. A. Munz, I.K. Iden, H. Johansen (2009), Fluid-solid interations related to subsurface storage of CO_2 Experimental tests of well cement, *Energy Procedia*, 1, 3367 – 3374.

Chadwick, R.A., Marchant, B.P. & Williams, G.A. 2014. CO_2 storage monitoring: leakage detection and measurement in subsurface volumes from 3D seismic data at Sleipner. Energy Procedia (2013).

Fichler, C., et al. (2005), North Sea Quaternary morphology from seismic and magnetic data: indications for gas hydrates during glaciation?, *Petroleum Geoscience* 11(4), 331-337.

Flemisch, B et al. "DuMu^x: Dune for multi-{phase, component, scale, physics …} flow and transport in porous media. Advances in Water Resources 34,9 (2011):1102-1112"

Fossum, T. G., T. O. Sæbø, B. Langli, H. Callow, R. E. Hansen (2008), HISAS 1030 – High resolution interferometric synthetic aperture sonar, *Proceedings of CHC-NSC conference 2008*, Victoria, Canada.

Gutierrez, M., Øino, L.E. and Nygård, R. (2000), Stress-dependent permeability of a de-mineralised fracture in shale. Marine and Petroleum Geology, 17(8): 895-907.

Huuse, M., and H. Lykke-Andersen, (2000), Overdeepened Quaternary valleys in the eastern Danish North Sea: morphology and origin, *Quaternary Science Reviews 19.12*, 1233-1253.

Khajepor S., J. Wen & B. Chen 'Multi-pseudopotential interaction: a solution for thermodynamic inconsistency in pseudopotential lattice Boltzmann models' Phy. Rev. E. (under review)

Kristensen, T.B., Piotrowski, J.A., Huuse, M., Clausen, O.R. and Hamberg, L., (2008), Time-transgressive tunnel valley formation indicated by infill sediment structure, North Sea – the role of glaciohydraulic supercooling. Earth Surface Processes and Landforms, 33(4): 546-559.

Lonergan, L., Maidment, S.C.R. and Collier, J.S. (2006), Pleistocene subglacial tunnel valleys in the central North Sea basin: 3-D morphology and evolution. Journal of Quaternary Science, 21(8): 891-903.

Løseth, H., Wensaas, L., Arntsen, B., and Hanken, N. (2011), 1000 m long gas blow-out pipes: Marine and Petroleum.

Scherer, G.W., M.A. Celia, J-H. Prevost, S. Bachu, R. Bruant, A. Duguid, R. Fuller, S.E. Gasda, M. Radonjic, W. Vichit-Vadakan (2005), Leakage of CO_2 through abandoned wells: Role of corrosion of cement. In: S.M. Benson (ed), *Carbon dioxide capture for storage in deep geological formations – results from the CO_2 capture project, Elsevier*: Vol 2, 827-848.

Someya S.,B. Chen, et al, (2005) 'Measurement of CO_2 solubility in pure water and the pressure effect on it in the presence of clathrate hydrate", Int. J. of Heat & Mass Transfer, Vol. 48, 2503–2507

Praeg, D. (2003), Seismic imaging of mid-Pleistocene tunnel-valleys in the North Sea Basin—high resolution from low frequencies, *Journal of Applied Geophysics,* 53(4), 273-298.

Wie W. & B. Chen, 'A dissolution lattice Boltzmann model and the simulation of CO_2 dispersion and dissolution in porous channel', Phy. Rev. E. (to be submitted)

Appendix

Table 1: Summary of technologies and techniques used for monitoring CCS sites

Tool		Data type	Information derived	Strenghts	Weaknesses
Seafloor mapping	Multibeam echosounder	Bathymetry from the seafloor	• topographic map of the seafloor	• commercially available and present on many research vessels	• limits in the resolution
	HISAS	High-resolution images from the seafloor	• high-resolution topographic maps and high-resolution images of the seafloor • identification of irregular features at the seafloor	• commercially available AUV system • high area coverage rates given the resolution	• requires high navigational accuray • surface properties can influence the systems range and reception
Seismic	Regional seismology	• Records of earthquake magnitues, locactions and depth • Maximunm ground motion velocities and displacements	• background levels of natural seismicity • magnitude and orientation of regional stress field	• low costs	• leads to very local datasets only
	Regional 2D seismic lines	Time and depth migrated seismic sections	• regional structural cross sections • lateral distance to subcrop/outcrop of foramtions • regional map of lateral continuity of the primary seal		
	Field specific 2D and 3D seismic	Time and depth migrated 2D sections and 3D volumes	• detailed structural imaging • location, orientation and throw of geological faults • 3D time and depth formation horizon maps • large-scale vertical and horizontal reservoir stratigraphic features, particlularly unconformities, erosional surfaces and heterogeneity • detailed, local map of lateral contiunity of the primary seal.	• Covering large areas in a cost efficient way • requires high navigational accuray • leads to very detailed maps	• requires large survey campaigns • cost can be high
Fluid Flow Modeling	DuMux	Geological model and reservoir parameters	CO_2 plume evolution and leakage rates	Open sources tool, available free	Research tool, requires expert knowledge to use. Do not have graphical user interface
Pore-scale LBM modeling	Lattice Boltzmann Method	• Non-Darcy's law model • In-house computer code written by Fortran	• New thermodynamic inconsistency LBM developed to handle large density ratio • A in-house code of two-phase flow LBM by Fortran was developed • A model of CO_2 dissolution of both the free-rising droplet and the flow in pore-channel was developed • An effective grid-mapping method was adapted to the code design, which enhanced the resolution.	•Model code is easy to be improved further to model the multi-phase and multi-components flow in porous media. • To be available to developed for parallel computation. • To be commercialized further.	• Users are requested to understand the theories of LBM
	heterogeneities porous sediments	Digital data of of sediments /geoformation	• Digital reconstructed porous sediments/geoformation	• Simulation of two-phase flow through different structures of the sediments and cap racks.	• requires digital data of porous sediments
	two-phase flow	CO2 (gas or liquid)/brine	• Dispersion rate of CO2 (gas/liquid) through the porous sediments • Dissolution rate of CO2 (gas/liquid) through the porous sediments • Effects of heterogeneity (the reconstructed geoformation) on CO2 dispersion and dissolution	• Simulation and prediction of the multi-phase and multi-components flows in porous sediments. • A relatively stable numerical scheme to model the multi-phase flows with large density ratio.	• Best applications to the theoretical and mechanism studies within the pore and laboratory scales